Delineation of the healthy rabbit kidney by immunohistochemistry - A technical note.

Meier Bürgisser, Gabriella ; Heuberger, Dorothea M ; Giovanoli, Pietro ; Calcagni, Maurizio ; Buschmann, Johanna

Abstract: Pre-clinical animal models are needed to investigate and study kidney injuries and diseases. The rabbit kidney model is frequently used because various important parameters can be assessed with it. For example, histology and immunohistochemistry are indispensable as tissue morphology and composition can be investigated qualitatively as well as quantitatively. Here, different histological and immunohistochemical stainings were performed in the rabbit healthy naïve kidney tissue. First, overnight formalin fixation followed by paraffin embedding and cryopreservation with a subsequent 10-minute formalin fixation prior to staining were compared. Cryosections showed a more pronounced staining pattern, with clear borders at low magnifications, but blurred borders at higher magnifications. Then, antigen retrieval (AR) for paraffin embedded sections resulted in more prominent corresponding signals compared to stainings without AR. Moreover, several advantages and disadvantages of chromogenic versus immunofluorescence stainings were considered. Chromogenic staining was advantageous compared to immunofluorescence for collagen I and III, and to a minor degree for fibronectin. Finally, distinct structures, such as the pelvis, the calices, the glomeruli and tubuli, were stained in serial sections with diverse immunohistochemical stainings in order to delineate their composition. The following stainings were performed: standard HaematoxylinEosin and Elastica van Gieson staining, collagen I, collagen III, fibronectin, -SMA, ki-67 and protease-activated receptor-2 (PAR-2). While chromogenic stainings of collagen I and collagen III were particularly useful to depict kidney structures in paraffin sections compared with cryosections, cryosections immunofluorescently stained for -SMA were superior to paraffin sections, particularly at higher magnifications. With regard to specific structures, we found renal vessel walls positive for fibronectin and -SMA, while the Bowman's capsule was only positive for fibronectin and -SMA showed only tiny spots. The mesangial cells of the glomeruli and the distal tubuli were PAR-2 positive, while the proximal tubuli were PAR-2 negative.

DOI: https://doi.org/10.1016/j.acthis.2021.151701

Originally published at:
Meier Bürgisser, Gabriella; Heuberger, Dorothea M; Giovanoli, Pietro; Calcagni, Maurizio; Buschmann, Johanna (2021). Delineation of the healthy rabbit kidney by immunohistochemistry - A technical note. Acta Histochemica, 123(4):151701.
DOI: https://doi.org/10.1016/j.acthis.2021.151701

Acta Histochemica 123 (2021) 151701

Contents lists available at ScienceDirect

Acta Histochemica

journal homepage: www.elsevier.com/locate/acthis

Delineation of the healthy rabbit kidney by immunohistochemistry – A technical note

Gabriella Meier Bürgisser [a], Dorothea M. Heuberger [b], Pietro Giovanoli [a], Maurizio Calcagni [a], Johanna Buschmann [a,*]

[a] Division of Plastic Surgery and Hand Surgery, University Hospital Zurich, Sternwartstrasse 14, Zurich, 8091, Switzerland
[b] Institute of Intensive Care Medicine, University Hospital Zurich, Sternwartstrasse 14, Zurich, 8091, Switzerland

ARTICLE INFO

Keywords:
Cryosection
Antigen retrieval
Immunofluorescence
Bowman's capsule
Tubulus
Renal corpuscle

ABSTRACT

Pre-clinical animal models are needed to investigate and study kidney injuries and diseases. The rabbit kidney model is frequently used because various important parameters can be assessed with it. For example, histology and immunohistochemistry are indispensable as tissue morphology and composition can be investigated qualitatively as well as quantitatively. Here, different histological and immunohistochemical stainings were performed in the rabbit healthy naïve kidney tissue. First, overnight formalin fixation followed by paraffin embedding and cryopreservation with a subsequent 10-minute formalin fixation prior to staining were compared. Cryosections showed a more pronounced staining pattern, with clear borders at low magnifications, but blurred borders at higher magnifications. Then, antigen retrieval (AR) for paraffin embedded sections resulted in more prominent corresponding signals compared to stainings without AR. Moreover, several advantages and disadvantages of chromogenic versus immunofluorescence stainings were considered. Chromogenic staining was advantageous compared to immunofluorescence for collagen I and III, and to a minor degree for fibronectin. Finally, distinct structures, such as the pelvis, the calices, the glomeruli and tubuli, were stained in serial sections with diverse immunohistochemical stainings in order to delineate their composition. The following stainings were performed: standard Haematoxylin&Eosin and Elastica van Gieson staining, collagen I, collagen III, fibronectin, α-SMA, ki-67 and protease-activated receptor-2 (PAR-2). While chromogenic stainings of collagen I and collagen III were particularly useful to depict kidney structures in paraffin sections compared with cryosections, cryosections immunofluorescently stained for α-SMA were superior to paraffin sections, particularly at higher magnifications. With regard to specific structures, we found renal vessel walls positive for fibronectin and α-SMA, while the Bowman's capsule was only positive for fibronectin and α-SMA showed only tiny spots. The mesangial cells of the glomeruli and the distal tubuli were PAR-2 positive, while the proximal tubuli were PAR-2 negative.

1. Introduction

Renal diseases exhibit different aberrations of the kidney tissue, such as tubulointerstitial myofibroblast accumulation and fibrosis (Tang et al., 1996), glomerular injury (Alpers et al., 1994), prevalence of a calcifying endothelial phenotype in chronic kidney disease (Cianciolo et al., 2017) or kidney stones (Wang et al., 2020). In order to elucidate such diseases and determine pathological mechanisms in detail, pre-clinical animal models are needed. There are reports using mice to study polycystic kidney disease (Atwood et al., 2020), rats to elucidate acute kidney injury by clamping renal arteries or veins (Karami et al., 2020) and pigs to examine renal ischemia-reperfusion (Beach et al., 2020). Among these animal model, the rabbit kidney model has been reported to be successful to analyse specific drugs targeting kidney disease after endotoxic shock (Siddiqui et al., 2020) or to test immunodepressents after kidney transplantation (Saeed et al., 2020). However, changes in tissue composition analysed by histology and immunohistochemistry remain fragmentary. In most cases, selected stainings are provided, focused on the kidney disease under view.

Here, we provide a technical note aiming to give an overview of a series of different typical stainings of the healthy kidney tissue. Directing the reader to the optimum fixation and staining techniques for typical

* Corresponding author at: University Hospital Zurich, ZKF, Division of Plastic Surgery and Hand Surgery, Sternwartstrasse 14, Zurich, 8091, Switzerland.
E-mail address: johanna.buschmann@usz.ch (J. Buschmann).

https://doi.org/10.1016/j.acthis.2021.151701
Received 2 December 2020; Received in revised form 26 February 2021; Accepted 26 February 2021
Available online 7 March 2021

kidney (sub) structures, we discuss basic aspects of paraffin tissue sections fixed with formaldehyde compare them to cryopreservation. Furthermore, we show the advantage of an additional antigen retrieval (AR) step compared to immunohistochemical staining without AR for paraffin sections. Finally, we compare chromogenic versus fluorescence staining, respectively, by providing serial sections and the same location of the regions of interest.

Like this, we have assessed Haematoxylin&Eosin (HE) and Elastica van Gieson (EvG) staining in the healthy rabbit kidney tissue, as well as collagen I, collagen III, fibronectin, alpha smooth muscle actin (α-SMA) and protease-activated receptor-2 (PAR-2) staining. The marker PAR-2 is an inflammation related protein on the cell surface, potentially interesting in studies of crescentic glomerulonephritis (Cunningham et al., 2000; Moussa et al., 2007), in ischemia-reperfusion kidney injuries (El Eter and Aldrees, 2012) or podocytes injury as induced by thrombin (Sharma et al., 2017). Moreover, renal PAR-2 was shown to be involved in the control of blood pressure in rats (Morla et al., 2013).

In addition, we chose specific morphological structures, such as the renal pelvis, the calices, the cortex and medulla, as well as the glomeruli, the tubuli the Henle's loops and Bertin columns with different stainings to elucidate the local composition of these structures in a qualitative, descriptive and for certain assessments in a semi-quantitative and quantitative way.

The data presented here can support researchers who intend to use the rabbit kidney model in choosing an appropriate staining to delineate a specific target structure. In addition, the results shown here provide a set of baseline or reference images helping other researchers who use the rabbit kidney model to compare their results. Finally, the images provided for the rabbit kidney here may prospectively be used also for inter species comparison, including the human kidney.

2. Materials and methods

2.1. Kidney extraction

A study of calvarial bone defects provided one fresh cadaver of a New Zealand White rabbit (female). The study had been approved by the Animal Ethics Committee of the local authorities (Canton Zurich ZH 108/2012 and 115/2015) (Ghayor and Weber, 2018; Siegenthaler et al., 2020). The whole kidney was extracted from this rabbit body, then stored on ice for a short time with subsequent processing for histology. All kidney sections were randomly selected.

2.2. Histology and immunohistochemistry

For either paraffin embedding or cryopreservation, the kidney pieces were halved. After that, the pieces for paraffin embedding were fixed in formalin for one day, dehydrated, paraffin-embedded and sectioned into 5-μm-thick slices. Prior to any histological staining, paraffin embedded sections were deparaffinized with xylene and rehydrated (descending gradient of ethanol).

As for the cryopreservation all pieces were embedded in Tissue-Tek® O.C.T. (Sakura, Alphen aan den Rijn, The Netherlands, Europe). After that, they were frozen according to commonly established procedure before cryosections of 5-μm-thick slices were fabricated. These sections were fixed with formalin for 10 min after being thawed, and washed with 1xTBS followed by IHC procedures (next paragraph).

Elastica van Gieson (EvG) and Haematoxylin&Eosin (HE) staining was performed according to commonly established procedures. For immunohistochemistry and paraffin sections, an antigen retrieval (AR) step was performed in 10 mM citrate buffer (pH 6.0) with 0.05 % Tween-20 for 20 min at 95 °C. For some selected stainings no AR was performed for technical reason and control management, in order to visualize the staining without AR and show the differences provoked by this step. Depending on the epitope to stain, paraffin and cryosections were permeabilized with 0.5 % Triton X-100 in 1xTBS for 10 min and then washed three times with 1xTBS. After that, the sections were blocked in 5 % donkey serum and 1 % BSA in 1xTBS for 1 h (room temperature). Next, sections were incubated with mouse anti-collagen I antibody (ab90395; Abcam, Lucerne, Switzerland, 1 : 200 dilution) or mouse anti-collagen III antibody (AF5810; Acris, Wettingen, Switzerland, 1 : 200 dilution) or mouse anti-αSMA antibody (A2547; Sigma-Aldrich, Buchs, Switzerland, 1 : 500 dilution) or mouse anti-fibronectin antibody (F0791; Sigma-Aldrich, Buchs, Switzerland, 1 : 200 dilution) or mouse anti-ki67 antibody (NBP2-22112; Novus Biologicals, 1 : 500 dilution) or mouse anti-PAR-2 antibody (Santa Cruz Biotechnology, sc-13504 (SAM11), 1:250 dilution) on Refine-kit (anti-Rabbit-Polymer) and histofine-Mouse Polymer (1:50 dilution) diluted in 3 % BSA in 1xTBS overnight at 4 °C (Table 1). Laboratory validation of PAR-2 antibody has been reported previously (Meier Bürgisser et al., 2020). Briefly, the laboratory validation consisted of showing the *specificity* of PAR-2 antibody for rabbit tissue (exemplified in rabbit tongue and brain tissue) as well as the *reproducibility* of PAR-2 staining (exemplified in a series of rabbit Achilles tendon tissues, stained at different time points, i.e. 3, 6 and 12 weeks, respectively, and with different lots of the antibody). Further information can be found in the supporting information of our previous report (Meier Bürgisser et al., 2020). As a negative control, Normal Mouse Serum Control (08-6599, Invitrogen, no dilution) was used and sections were incubated with it overnight at 4 °C, too.

Table 1
Antibodies and conditions for IHC stainings.

Primary antibody	Source	Dilution
mouse anti-collagen I	ab90395; Abcam, Lucerne, Switzerland	1 : 200
mouse anti-collagen III	AF5810; Acris, Wettingen, Switzerland	1 : 200
mouse anti-αSMA	A2547; Sigma-Aldrich, Buchs, Switzerland	1 : 500
mouse anti-fibronectin	F0791; Sigma-Aldrich, Buchs, Switzerland	1 : 200
mouse anti-ki67	NBP2-22112; Novus Biologicals	1 : 500
mouse anti-PAR-2	Santa Cruz Biotechnology, sc-13504 (SAM11) on Refine-kit (anti-Rabbit-Polymer) and histofine-Mouse Polymer	1 : 250 1 : 50
Normal Mouse Serum	08-6599, Invitrogen	no dilution

Fluorescent immunohistochemistry was performed for collagen I and III, fibronectin and α-SMA, respectively, and chromogenic immunohistochemistry was performed for collagen I and III, fibronectin, ki67 and PAR-2, respectively. For fluorescent immunohistochemistry, primary antibody solution was removed and samples were washed with 1xTBS before incubation with secondary donkey antimouse Alexa-488 antibody (A-21202; Invitrogen, Basel, Switzerland, 1:500 dilution) and 10 μg/mL 4′6-diamidino-2-phenylindole dilactate (DAPI) (Sigma-Aldrich, Switzerland) diluted in 3 % BSA in 1xTBS for 1 h at room temperature. Then, the slides were washed in 1xTBS and mounted using Dako Fluorescence Mounting Medium (Agilent, Basel, Switzerland).

Samples were blocked with 3 % hydrogen peroxide solution in water for 10 min (room temperature) for chromogenic immunohistochemistry and subsequently washed 3x with 1xTBS. Primary antibody detection was performed using a biotinylated anti-mouse IgG secondary antibody and streptavidin-horseradish peroxidase (HRP) (ZytoChem Plus HRP Kit Mouse; Zytomed Systems, Muttenz, Switzerland), followed by colorimetric detection according to the manufacturer's protocol using DAB substrate (DAB Substrate Kit High Contrast; Zytomed Systems, Germany). Finally, slides were washed in tap water and mounted using Faramount Aqueous Mounting Medium (Agilent).

Images of whole tissue sections were produced with a slide scanner (Pannoramic 250 Flash II, 3Dhistech, Budapest, Hungary). With CaseViewer-Sofware v.2.1 snapshots of fields of view were then taken, or alternatively imaged with a Leica 6000 light microscope (Leica, Basel,

Table 2
Overview of markers, techniques and stainings used in this study. Key: ECM = Extracellular Matrix, Chro = Chromogenic detection, Fluo = Immunofluorescence, AR = antigen retrieval. Note: for Fibronectin and Mouse Isotype negative control (NC) images with and without AR-step are shown; "AR" and "no AR" is mentioned on these images and AR was only performed in paraffin sections. For all other stainings on paraffin sections there is no mention about AR, but AR was applied.

Marker	Description	Embedding	AR	Staining
Collagen I (Col I)	Structural protein in ECM	Para + cryo	Yes	Chro + Fluo
Collagen III (Col III)	Structural protein in ECM	Para + cryo	Yes	Chro + Fluo
Fibronectin (Fn)	Glycoprotein for network building of the ECM	Para + cryo	Yes + No	Chro + Fluo
alpha smooth muscle actin (α-SMA)	Contractile smooth muscle fibres in ECM	Para + cryo	Yes	Fluo
ki67	Cell nucleus protein expressed in proliferating cells	Para + cryo	Yes	Chro
PAR-2	Inflammation-related protein on cell surface	Para	Yes	Chro
Elastin (EvG)	Elastic fibers in vessel walls	Para	(classical histology)	(classical histology)
HE	Most structures for comprehensive structural overview	Para	(classical histology)	(classical histology)

Switzerland).

All techniques and stainings used in this study are summarized in Table 2.

2.3. Statistical analysis

Data were analysed with IBM SPSS Statistics 26 software. Contingency table analysis was performed for nominal data (scores with five levels, i.e. 1; 1.5; 2; 2.5 and 3). Pearson contingency coefficients were computed as well as p values, corresponding to the null hypothesis that both kind of sections (paraffin and cryo) or both processing steps (antigen retrieval (AR) or no AR), respectively, exhibit each feature to the same degree. The p values were indicated for pairs that were significantly different, meaning if $p < 0.05$.

3. Results and discussion

3.1. Cryopreservation versus formalin fixation

The first step towards a successfully stained tissue section is the choice of an appropriate fixative. It has been shown that the same immunohistochemical staining results in different images of the stained sections if either fixation by formalin, acetic acid, paraformaldehyde-lysine-periodate or bouin had been performed before (Salguero et al., 2001). The reason for this different outcome is found in the different ability of the fixative to permeabilize the cells, meaning to partially break down the cell membranes and thus to allow the antibody the access to antigens located not only the cell surface, but also within the cells. Moreover, besides the membrane destruction, different fixatives also lead to differently stabilized enzymes, with partially denatured proteins, ending up in an overall differently looking image of the corresponding antibody-antigen staining.

In our technical study presented here, we used the healthy rabbit kidney tissue and compared formalin fixed and paraffin embedded sections (brief: paraffin sections) with cryosections of cryopreserved kidney tissue. The hypothesis was that cryopreserved tissue would retain the selected antigens better than the paraffin sections. However, a closer look at the higher magnifications revealed distinct advantages of the paraffin sections over cryosections. In Figs. 1–4, we compared paraffin versus cryosections; for collagen I, collagen III, ki67 and α-SMA immunohistochemical stainings, respectively.

As can be seen in the collagen I stained sections with DAB as chromogen, distinct morphologies of the Bowman's capsules und glomeruli as well as arterioles are depicted with a high contrast in cryosections compared to paraffin sections (Fig. 1). While for the paraffin sections, collagen I staining showed some background, staining the cell nuclei with a blue/brown colour mixture, cryosections had the brown colour from DAB in a clearer and more specific way, and cell nuclei were not stained brown here. Like this, localization of the Bowman's capsules with distinct Bowman's spaces are easy to be recognized at low magnification (upper row, Fig. 1). In contrast, at higher magnification, the brown, very intensive colour observed in the cryopreserved sections was a bit slurry with margins blurred so that the borders of the different morphological structures were not so clear as denoted in the paraffin sections. Hence, the advantage of the paraffin sections over the cryosections can be seen only at higher magnification, if closer inspection of structural details is necessary for tissue analyses. With very high magnification cryopreservation gives better details of structures.

Very similar to the findings for collagen I staining, collagen III immunohistochemistry of cryosections showed a much more pronounced staining pattern throughout the structures under view, with clear borders at low magnifications and blurred borders at higher magnifications. For paraffin sections, however, there was only a weak and partially unspecific staining, except for a Bowman's capsule at the border of a calix (see enlarged bottom row, Fig. 2). There, the surrounding tissue was clearly stained brown for collagen III in the extracellular matrix (ECM).

As for ki67 immunohistochemical staining, paraffin and cryosections looked quite different in their overall colour, with blueish for paraffin and brownish for cryosections, respectively (Fig. 3). The few proliferating cells, stained dark by ki67 antibody, however, were visible very well in paraffin sections, particularly at higher magnifications. In contrast, practically every cell was stained dark brown in the cryosections. There was obviously unspecific brown staining in these sections. The extracellular matrix was also stained brown. Therefore, rabbit kidney ki67 staining and proliferating cells would be overestimated in cryosections. We recommend paraffin sections with an AR for ki67 assessment in rabbit kidney tissue.

For α-SMA staining and immunofluorescence detection, the colour intensity (green) was higher in paraffin sections compared with cryosections (Fig. 4). This resulted in a more distinctive and precise staining that was α-SMA positive at higher magnification for cryosections. In contrast to paraffin sections where the green colour superimposed blue DAPI cell nuclei staining at the border of Bowman's capsules, the cryosections allowed a specific localization of α-SMA positive cells in the corresponding morphologies at higher magnifications, as assessed semi-quantitatively. Therefore, depending on the focus of a certain study, different magnifications get different importance and prominence as a result of the initial fixation technique. Researchers should therefore be aware what could be expected for the different immunohistochemical stainings and their appearance after varying fixation methods.

3.2. Antigen retrieval in paraffin embedded sections

It is well-known that tissue preservation by formalin fixation with subsequent paraffin embedding can lead to a decreased immunoreactivity of specific antigens. In order to retrieve those antigens, different techniques have been developed during the last 30 years. Starting in 1991, antigen retrieval was reported to be successful through heating the paraffin sections (Shi et al., 1991). Besides this method, several other techniques, based on different chemical treatment, have been developed and are useful during daily histological practice (Shi et al., 2006, 2011).

As expected, an antigen retrieval step enhanced the signal intensity of the fibronectin antibody staining remarkably, which is demonstrated

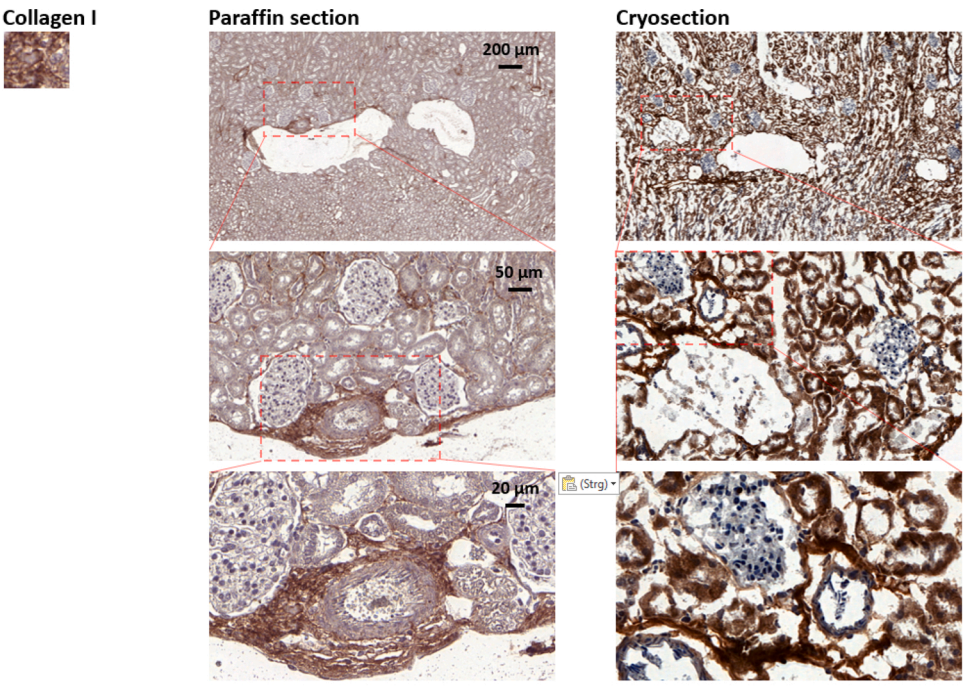

Fig. 1. Collagen I immunoshistochemical staining with DAB as chromogen (brown colour) for paraffin sections with AR (left) and for cryosections (right). Corresponding inserts (red dashed line) depict area used for images at the next lower level with higher magnification. Below: Contingeny tables for collagen I scores (1; 1.5; 2; 2.5;3) for brown intensity and for structure contrast and sharpness (n = 15 technical replicates for paraffin and cryosections, respectively; with 5 Fields of Views (FOVs) in the connective tissue, the tubular tissue and the artery wall, respectively). Definition of FOVs and scores is given in the Supporting Information Fig. SI 1. (For interpretation of the references to colour in this figure legend, the reader is referred to the web version of this article.)

Collagen I Brown intensity						
Score / *Section*	*1*	*1.5*	*2*	*2.5*	*3*	*Total*
Paraffin	3	8	4	0	0	15
Cryo	0	5	5	4	1	15
Total	3	13	9	4	1	30

Contingency coefficient (Pearson): 0.476; p = 0.066 (no significant difference between paraffin and cryo)

Collagen I Contrast and Sharpness						
Score / *Section*	*1*	*1.5*	*2*	*2.5*	*3*	*Total*
Paraffin	11	4	0	0	0	15
Cryo	0	4	7	4	0	15
Total	11	8	7	4	0	30

Contingency coefficient (Pearson): 0.650; p = 0.001 (significant difference between paraffin and cryo)

in Fig. 5. While the fibronectin positive structures in the paraffin sections can be well distinguished after an antigen retrieval step, such as the borders of arteries and tubules as well as Bowman's capsules, the same staining without AR does not reveal any useful morphologies. In addition, when we used mouse isotype fluorescence immunohistochemistry to show a negative control, the effect of an AR step was also obvious. While diverse microstructures can be well distinguished in the section treated with an AR step, practically nothing is exhibited in the corresponding sections stained without AR. Signal intensity was significantly enhanced by AR compared with sections treated without AR.

3.3. *Bright field imaging versus immunofluorescence*

As a further decision step in getting optimum histological images of the rabbit kidney, we compared bright field imaging of the brown colour with DAB as chromogen, with immunofluorescence. For both selected

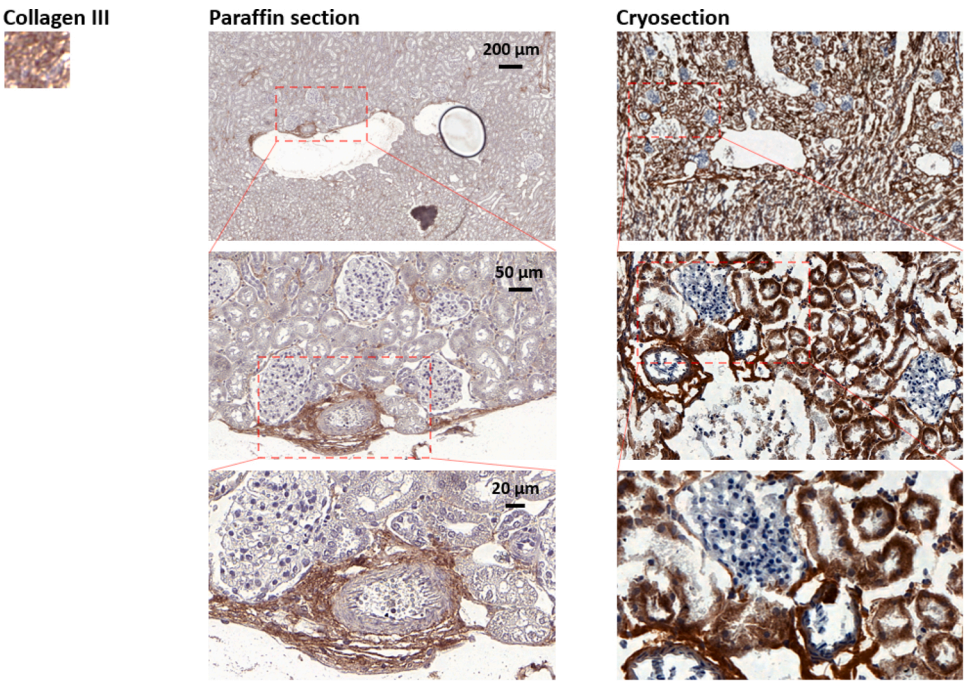

Fig. 2. Collagen III immunoshistochemical staining with DAB as chromogen (dark brown colour) for paraffin sections with AR (left) and for cryosections (right). Corresponding inserts (red dashed line) depict area used for images at the next lower level.
Below: Contingeny tables for collagen III scores (1; 1.5; 2; 2.5;3) for brown intensity and structure contrast and sharpness (n = 15 technical replicates for paraffin and cryosections, respectively; with 5 Fields of Views (FOVs) in the connective tissue, the tubular tissue and the artery wall, respectively). Definition of Field of Views and scores is given in the Supporting Information Fig. SI 2. (For interpretation of the references to colour in this figure legend, the reader is referred to the web version of this article.)

Collagen III Brown intensity						
Score / *Section*	*1*	*1.5*	*2*	*2.5*	*3*	*Total*
Paraffin	7	3	4	1	0	15
Cryo	0	5	6	1	3	15
Total	7	8	10	2	3	30

Contingency coefficient (Pearson): 0.516; p = 0.028 (significant difference)

Collagen III Contrast and Sharpness						
Score / *Section*	*1*	*1.5*	*2*	*2.5*	*3*	*Total*
Paraffin	9	6	0	0	0	15
Cryo	2	7	2	2	2	15
Total	11	13	2	2	2	30

Contingency coefficient (Pearson): 0.510; p = 0.032 (significant difference)

markers of the ECM, collagen I and collagen III, we found that bright field imaging was advantageous compared to immunofluorescence (Fig. 6). The structures and substructures were visible better and small entities, such as tubuli and capsules, could be distinguished from each other better than in the corresponding immunofluorescence stained sections. However, as shows the following, this might depend on the antibody under use. For example, if fibronectin staining was compared between bright field and fluorescence, the advantage of bright field over fluorescence was not so pronounced as had been found for collagen I and III. Here, the DAB staining with subsequent bright field imaging revealed the fibronectin positive areas quite good, as good as the immunofluorescent staining. But at some few locations, the DAB staining showed it even less well, caused by an increased background staining, which resulted in spots with very dark brown staining and a slurry of colour in their proximity. We conclude from these findings that the decision for either DAB as chromogen or immunofluorescence depends on the antibody under view, but might lead to significant differences in the distinction of precise structures. Noteworthy to mention, fast optical colour loss occurring typically in fluorescent sections or inadequate scanning by digital microscopic devices have to be considered, too.

3.4. Anatomy of the rabbit kidney

An overview of a typical healthy rabbit kidney tissue is given in Fig. 7A. The α-SMA positive areas reveal the two main regions of the kidney, the *cortex* with its border (*capsula*) and the *medulla*, respectively.

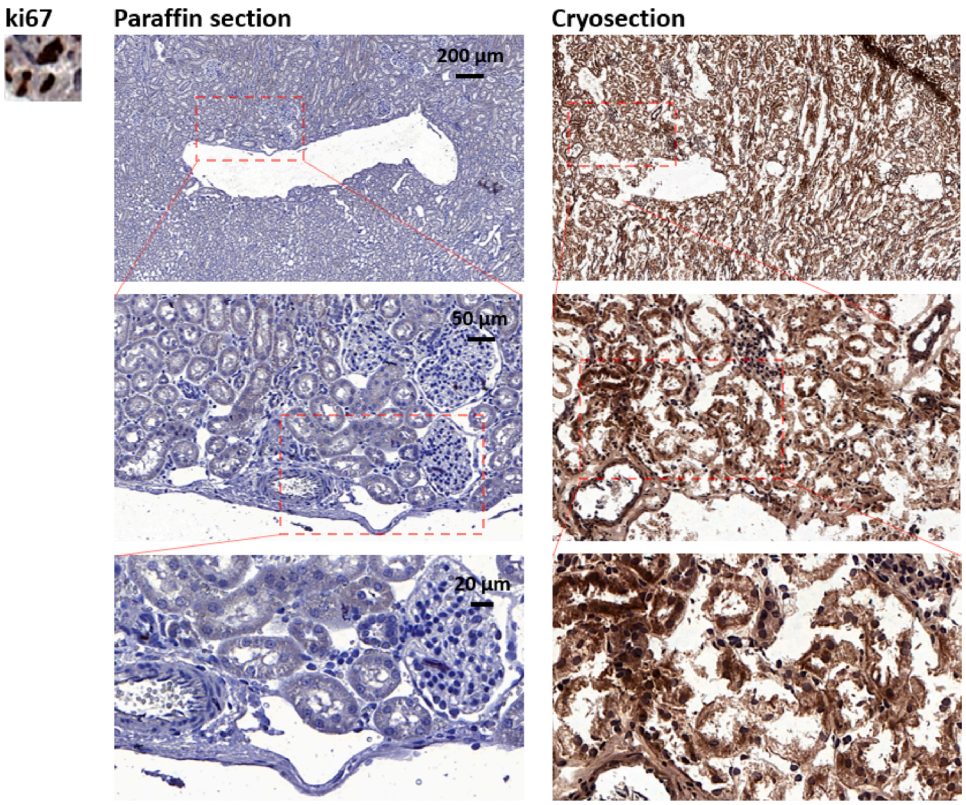

Fig. 3. Ki67 immunoshistochemical staining with DAB as chromogen (dark brown colour) for paraffin sections with AR (left) and for cryosections (right). Corresponding inserts (red dashed line) depict area used for images at the next lower level. (For interpretation of the references to colour in this figure legend, the reader is referred to the web version of this article.)

While 90 % of the blood flows through the cortex, only 10 % flows through the medulla. Typical structures for arteries with their thick α-SMA positive walls as well as veins with rather thinner α-SMA positive walls can be distinguished well in the cortex. Moreover, *calices*, *papillae* and renal columns (*Bertini* columns) are depicted in the magnified region.

In Fig. 7B and C, diverse anatomical structures are shown in H&E stained sections and corresponding subsequent sections stained for PAR-2. PAR-2 staining might be interesting to localize inflammation and pain within the renal system. In the H&E stained sections, which is the golden standard of histological staining, the renal corpuscle with its Bowman's capsule, the Bowman's space to collect the primary urine, its podocytes are very well distinguishable. In addition, arteries with erythrocytes and myocytes in the vessel wall can also be seen quite well. Interestingly, when PAR-2 staining is locally analysed, the proximal tubuli are weakly stained, while the distal tubuli are clearly PAR-2 positive, which stands in contrast to human proximal tubuli that were reported to prominently express PAR-2 (Vesey et al., 2013). Moreover, the intermediary rabbit tubuli were completely PAR-2 negative. Such histological findings could be useful for the discussion of cases with distal renal acidosis (Tekçe et al., 2013), where symptoms similar to typical coronary diseases might lead to unnecessary coronary interventions despite the (hidden) kidney problem. Furthermore, the intra-renal distribution of PAR-2 protein expression, with none in the proximal and very clear expression in the distal tubuli, could also be correlated to ghrelin overexpression in diabetic individuals as well as animal models with the aim to relate inflammatory and growth hormone expression in renal research (Kuloglu and Dabak, 2009). Co-localization of ghrelin immunoreactivity and PAR-2 expression might elucidate or complete fragmentary trigger pathways for diabetes mellitus. Nevertheless, it has to be emphasized that one should be careful to translate these findings for the rabbit kidney to the human kidney, particularly in conclusions about signalling pathways.

Moreover, in Fig. 7C, a typical Bowman's capsule is shown; the vascular pole with its *vas afferens* and *vas efferens*, as well as the urinary pole are marked. The parietal sheet of the Bowman's capsule as well as its visceral sheet with the podocytes are delineated clearly. The proximal convoluted tubulus and the distal convoluted tubulus can be seen on the right side of the image. In the PAR-2 stained sections, the marked difference between signal intensity in cells attributed to the distal tubulus compared with the proximal tubulus is obvious – as in Fig. 7B, endothelial cells in the proximal tubulus are practically PAR-2 negative and cells from the distal tubulus dark brown. Such a difference in PAR-2 staining was also observed between mesangial cells in the mesangium of the Bowman's capsule compared with juxtaglomerular cells at the rim of the capsule; mesangial cells stained dark brown, while juxtaglomerular and even more pronounced the extraglomerular mesangial cells were only very weakly stained for PAR-2. If such intra-renal PAR-2 distribution has any consequences or implications in terms of inflammatory response in chronic kidney failure or other kidney related diseases, was not described up-to-date. To the best of our knowledge, this is the first report on intra-renal PAR-2 distribution in the healthy rabbit kidney. Different transport and exchange processes occurring via the walls of the renal tubuli take place at different parts of the tubuli and are based on different cell types in the tubulus walls; channels to keep salt, water or proton activity within the physiological range demand for different cell types and differently constructed channels through the tubular walls than do for example processes to eliminate metabolic end products or foreign molecules. Hence, it might be speculated that there is a relation between PAR-2 expression with a specific inflammatory sensitivity in the distal tubulus with the convenient function to re-absorb glucose or amino acids. Likewise, a specific inflammatory sensitivity attributed to the mesangial cells within the Bowman's capsule could be correlated to a certain inflammation-related signalling function, which

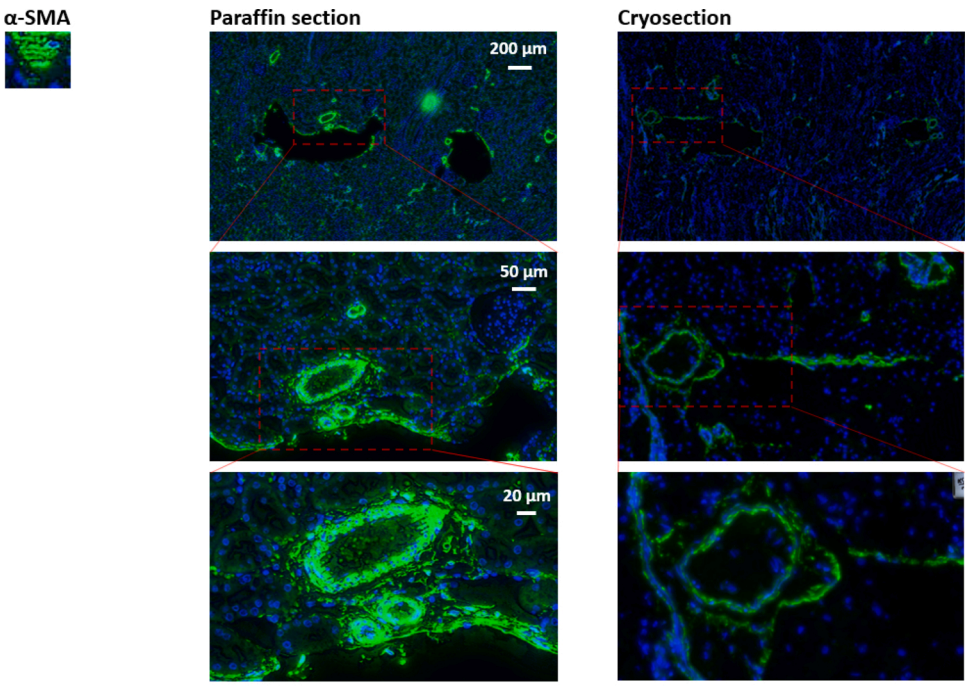

Fig. 4. Immunohistochemical α-SMA staining with immunofluorescence detection. α-SMA (light green) and cell nuclei (DAPI staining, blue) can be seen in paraffin sections with AR (left) and for cryosections (right). Corresponding inserts (red dashed line) depict area used for images at the next lower level with higher magnification. Below: Contingeny table for α-SMA scores (1; 1.5; 2; 2.5;3) for green colour accuracy and staining (n = 5 technical replicates for paraffin and cryosections, respectively; (the 5 FOVs for paraffin and cryosection are defined in the Supporting Information Fig. SI 3). (For interpretation of the references to colour in this figure legend, the reader is referred to the web version of this article.)

α-SMA accuracy and staining						
Score	*1*	*1.5*	*2*	*2.5*	*3*	*Total*
Section						
Paraffin	0	0	3	2	0	5
Cryo	4	1	0	0	0	5
Total	4	1	3	2	0	10

Contingency coefficient (Pearson): 0.707; p = 0.019 (significant difference)

is absent in extraglomerular mesangial cells because unnecessary. It could therefore be useful for further studies to provide these images as baseline values, from which the pathological state can be discriminated.

3.5. Staining for different markers at the same place

Serial sections were taken and immunohistochemistry of a series of markers was performed at the same location. Fig. 8A gives an overview of a typical renal section, with the main components, the cortex and the medulla. While collagen I and III as well as fibronectin chromogenic staining did not reveal any particular substructures obviously, immunofluorescent staining for fibronectin and for α-SMA clearly showed the vessels and tubuli well at the chosen low magnification. Moreover, staining for PAR-2 depicted the glomeruli as well as the distal tubuli in the cortex very well, with increasing staining intensity towards the capsula. In this overview, the combination of consecutive sections stained for fibronectin, α-SMA and PAR-2 can therefore be judged to give representative insight into the morphological composition of a typical healthy rabbit kidney.

At higher magnification, as realized in Fig. 8B, the difference between collagen I and collagen III distribution can be seen better in the chromogenic stained sections compared with the immunofluorescent stained sections. For fibronectin on the other hand, both, the chromogenic and immunofluorescent stainings, depict the vessels and glomeruli very well. While fibronectin is not only positive in the walls of the vessels, but also in the walls of the Bowman's capsule, α-SMA stains positively only in the vessel wall, but not in the walls of the Bowman's capsule. This clear difference can be even better observed in Fig. 8C. Very clearly, the *adventitia* of the vessel wall is stained green in both, the fibronectin and α-SMA immunofluorescent stained sections. However, a look at the nearby glomerulus shows that only fibronectin is expressed around the capsule, but not α-SMA. This can be claimed for exactly the same glomerulus as sections were taken one after the other for this purpose. The findings for the different distribution of fibronectin and α-SMA make sense with regard to physiology because myofibroblast marker α-SMA expressing cells with their inherent contractibility are needed particularly in the walls of arteries, while the rim of the glomerulus (the Bowman's capsule) has no need to contract and is therefore α-SMA negative – under healthy conditions as used here. However, under pathological conditions, such as sclerotic lesions, a co-localization of Sox9 positive and α-SMA positive cells was reported in the cells forming the Bowman's capsule (Prochnicki et al., 2018). These findings were explained by fibrosis in the glomerular lesions. Interestingly, in the same study, α-SMA positive cells were also found in the glomerular tuft which is situated within the glomerulus, where under healthy conditions no α-SMA positive cells were detected.

A further marker studied here is ki67 for proliferating cells. It can be seen that the proliferating cells were more prominently found in the mesangial cells within the glomerulus compared with the cells making up the different parts of the tubuli. There, only very few cells were ki67 positive. The PAR-2 staining in the extract shown here confirms the findings mentioned for Fig. 7B and C, with PAR-2 positive mesangial

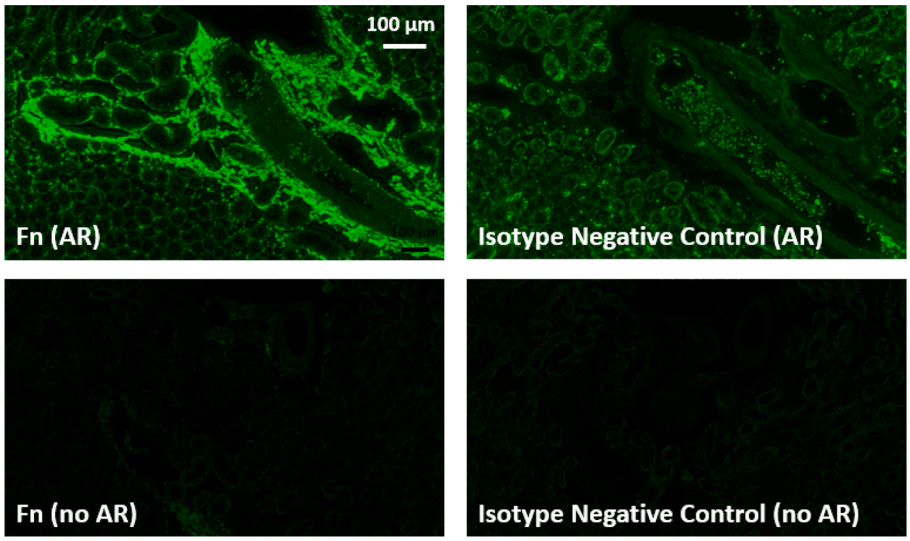

Fig. 5. Comparison of fibronectin immunofluoresence staining with antigen retrieval (AR) or without AR and Isotype negative controls in paraffin sections. Below: Contingeny tables for fibronectin scores (1; 1.5; 2; 2.5;3) for green colour intensity (n = 5 technical replicates for antigen retrieval and no AR, respectively, and for corresponding isotype negative controls. replicates with Details about location of the 5 FOVs for each condition are given in the Supporting Information Fig. SI 4. (For interpretation of the references to colour in this figure legend, the reader is referred to the web version of this article.)

Fibronectin green intensity						
Score *Antigen Retrieval (AR)*	*1*	*1.5*	*2*	*2.5*	*3*	*Total*
AR	0	0	0	0	5	5
no AR	0	3	1	1	0	5
Total	0	3	1	1	5	10

Contingency coefficient (Pearson): 0.707; p = 0.019 (significant difference)

Iso NC green intensity						
Score *Antigen Retrieval (AR)*	*1*	*1.5*	*2*	*2.5*	*3*	*Total*
AR	0	4	1	0	0	5
no AR	5	0	0	0	0	5
Total	5	4	1	0	0	10

Contingency coefficient (Pearson): 0.707; p = 0.007 (significant difference)

cells and endothelial cells of the distal tubulus, while extraglomerular cells and cells of the intermediary and proximal tubulus were PAR-2 negative.

In Fig. 9, collagen I, collagen III and α-SMA expression were assessed and compared in cryosections. While Fig. 9A shows the cortex and medulla and focuses on the calices, Fig. 9B depicts a glomerulus and some tubuli. The rim of the calices were α-SMA positive, however, at the highest magnification shown here, no α-SMA positive regions can be distinguished within the selected glomerulus. In contrast, at even higher magnification as realized in Fig. 10, the α-SMA stained section shows that there are also α-SMA positive regions within the glomerulus in the mesangium like in the interstitial peri-endothelial cells. As early as 1994, Alpers and co-workers who examined the myoid filaments in biospies of patients with glomerular injury, hypothesized that such

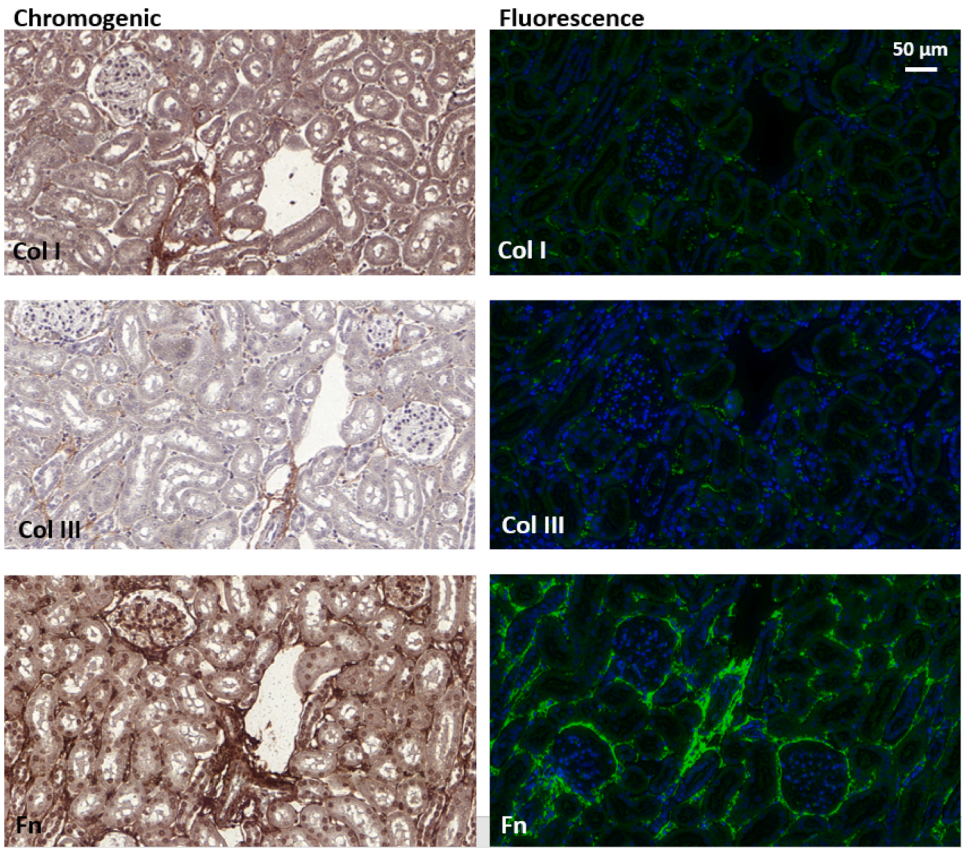

Fig. 6. Immunohistochemical staining for collagen I, collagen III and fibronectin for chromogenic staining and bright field imaging (left; DAB as chromogen) and immunofluorescence staining and imaging (right). All samples were paraffin embedded and stainings performed with AR.

α-SMA positive regions in the interstitium may lead to the whole kidney acting as a contractile organ: like this, the kidney could regulate to some extent the blood flow by adjusting the pressure of the interstitial regions on the vessels (Alpers et al., 1994). As can be clearly seen in Fig. 10, α-SMA positive regions in the interstitium only occur as spots and do not lead to longer connected filaments, neither do α-SMA positive cells form junctions as realized in the vessel walls (see for example Fig. 8C where a thick connected α-SMA positive region characterizes the vessel wall and the α-SMA positive cells are clearly connected to each other). We therefore judge the hypothesis of a whole organ contractility for the healthy kidney rather improbable. There might be some contractile elements found in the interstitium (with a hypothesized low functional influence), however, such α-SMA positive stromal cells are rather a sign for an eventual fibrosis and compromised renal function, as was reported earlier (Boukhalfa et al., 1996; Saratlija Novakovic et al., 2012). Particularly the α-SMA positive mesangial cells with myoid filaments occurring as tiny spots between healthy glomeruli would not support a reasonable functional role in terms of pressure regulation because vessels are only found at the vascular pole, outside the Bowman's capsule. In contrast, in glomerulonephritis, correlation between α-SMA levels expressed in glomeruli and in the interstitium resulted in positive correlation of high blood pressure and high α-SMA expression in the interstitium in children (Saratlija Novakovic et al., 2012). Moreover, in adult patients, higher α-SMA expression in glomeruli was associated with decreased serum creatinine, a waste product of the blood, resulting from muscle activity (Saratlija Novakovic et al., 2012). Under normal healthy conditions, creatinine is removed from the blood by the kidney, however, with more myoid filaments present and α-SMA expressing cells in the glomeruli, creatinine levels rise – a sign for impaired renal function.

3.6. Particular structures in the rabbit kidney

In Fig. 11, we present detailed structures of the glomerulus and the columns of Bertin, which are the medullary extensions of the renal cortex in between the renal pyramids. The overview at low magnifications with different stainings (Fig. 11A) shows that tubuli can be well recognized in paraffin sections with their positive chromogenic collagen I staining, while collagen III stained sections are mostly collagen III negative. The glomeruli are recognized well in the cryosections stained for collagen I and III (both DAB) because the mesangial cells are blueish and hence can be well distinguished from the deep brown staining of the corresponding collagen in the environment. Localization of the glomeruli is judged to be better in cryosections compared to paraffin sections.

As for PAR-2 staining, the tubuli and glomeruli can be seen very well because of their positive staining and the high contrast to the environment; with a deep brown colour, while the surrounding is mostly light brown or completely PAR-2 negative. Fig. 11B shows the magnifications of Fig. 11A. Here, one glomerulus is magnified and the different stainings can be compared. All immunofluorescently stained sections (paraffin: collagen I, collagen III, α-SMA; cryosection: α-SMA) show some spots of green colour, but the corresponding sections with chromogenic staining are to be favoured, particularly the paraffin embedded sections. For α-SMA, the paraffin sections at least show some positive areas in the glomerulus wall, while in the cryosections, α-SMA is completely negative throughout the excerpt. As for the ki67 stainings in paraffin and cryosections, both with chromogenic staining, the cryosections reveal the proliferating cells with a slightly higher contrast than the paraffin sections, however, in both kind of fixation techniques, the ki67 positive cells can be very well distinguished from the ki67 negative cells.

Next, Fig. 12 demonstrates different magnifications of the pelvis, the

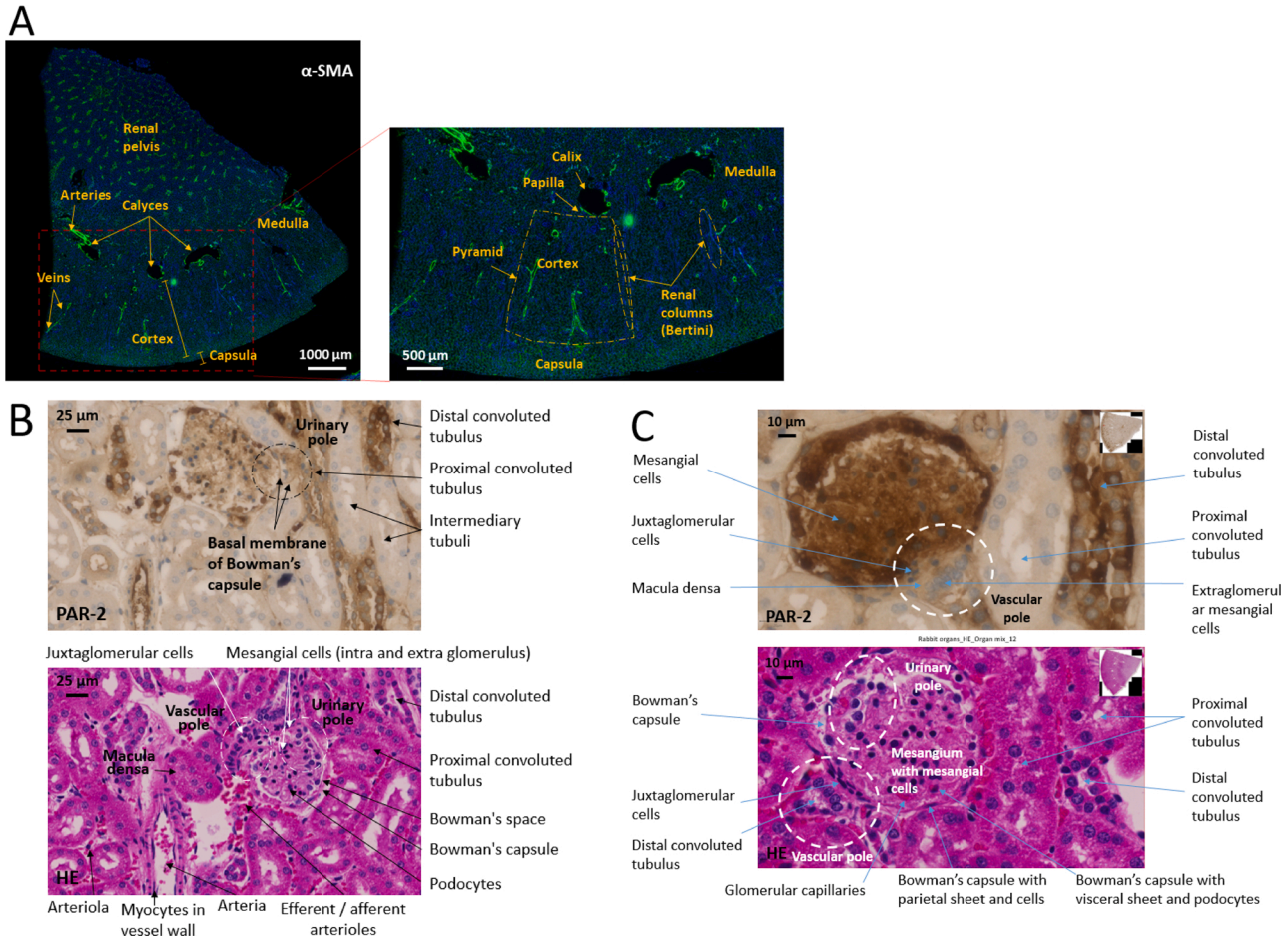

Fig. 7. Overview of a healthy rabbit kidney section immunohistochemically stained for α-SMA with AR (A) with corresponding tissue structures. Arrows depict specific substructures. PAR-2 and corresponding subsequent HE stained paraffin section (B and C) of specific parts of the renal system with detailed description of the substructures.

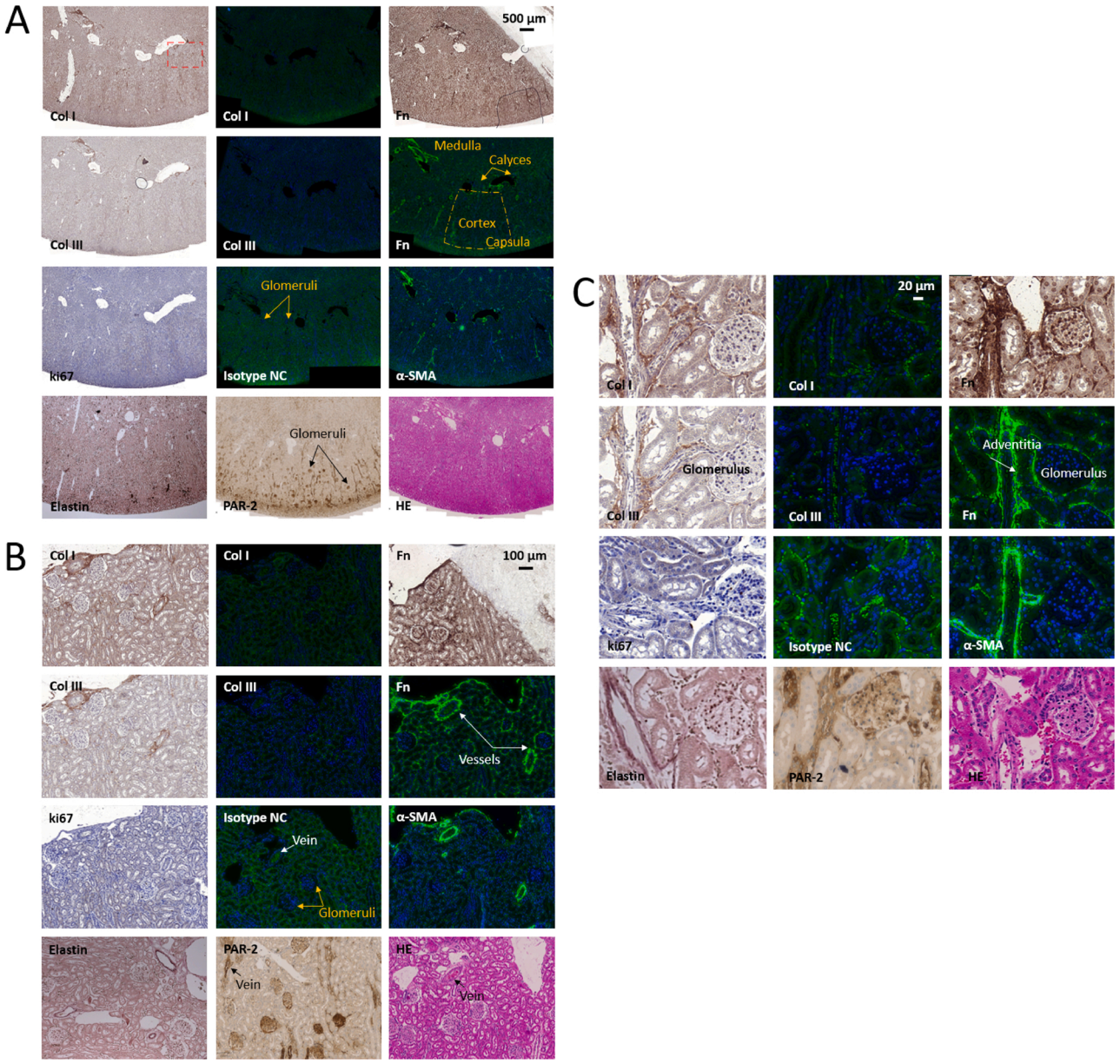

Fig. 8. Selected kidney tissue structures immunohistochemically stained for a series of different markers as well as Haematoxylin&Eosin and Elastica van Gieson for elastin at different magnifications in paraffin sections: Cortex with pyramids, calices and medulla (A); cortex with glomeruli, tubuli and blood vessels (B) and glomerulus, tubuli and vessels (C). *Key*: Col = Collagen, Fn = Fibronectin, Isotype NC = Mouse Isotype negative control, α-SMA = alpha smooth muscle actin, ki67 = proliferation marker ki67, PAR-2 = protease activated receptor-2 and HE = Haematoxylin&Eosin, AR = Antigen retrieval. If not otherwise stated, all stainings were performed with AR.

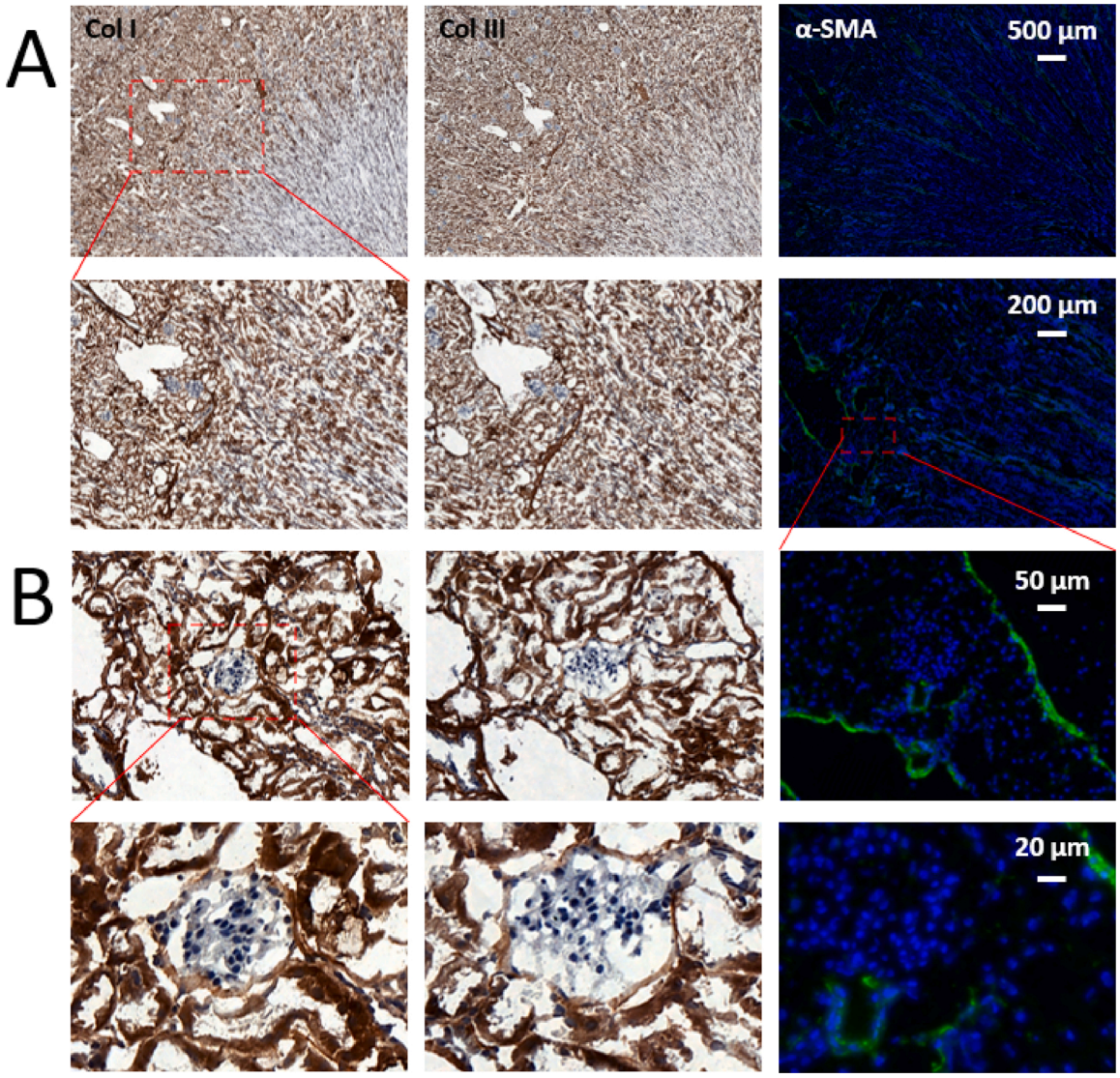

Fig. 9. Selected kidney tissue structures immunohistochemically stained for a series of different markers at different magnifications in cryosections: Cortex, medulla and calices (A); glomerulus and tubuli (B). *Key*: Col = Collagen, α-SMA = alpha smooth muscle actin.

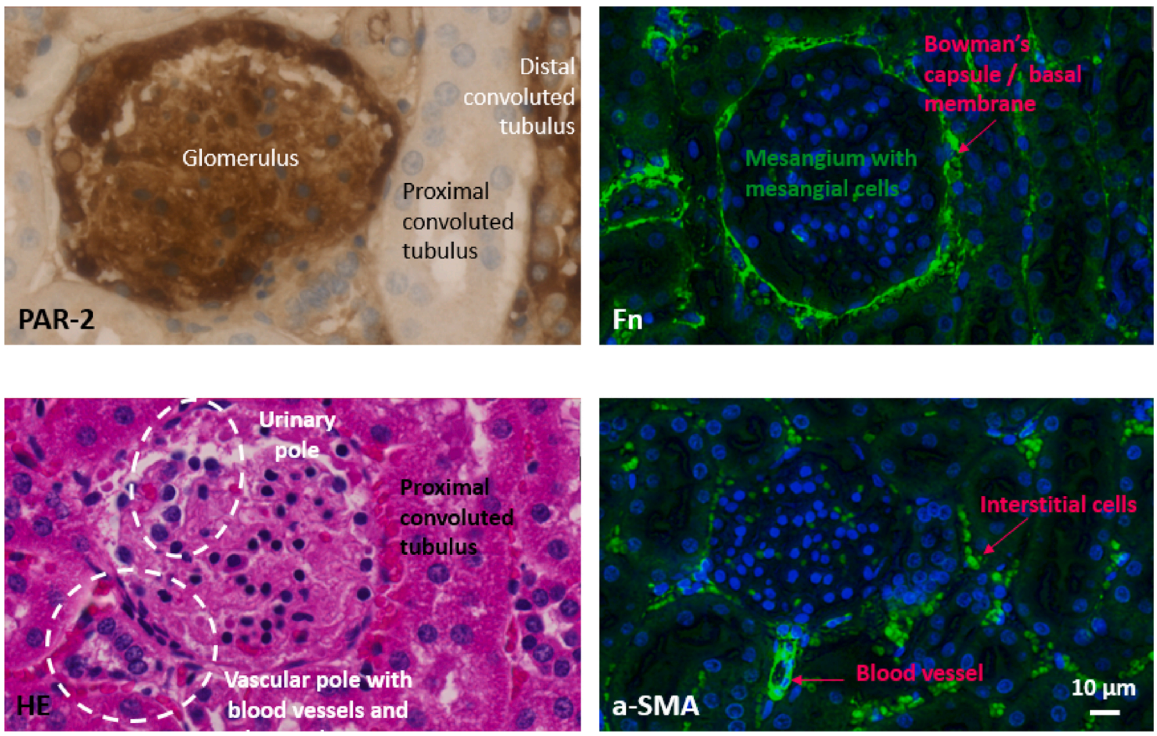

Fig. 10. The renal corpuscle – ultrastructural localization of PAR-2, fibronectin and α-SMA expression. *Key*: PAR-2 = protease activated receptor-2, Fn = Fibronectin, HE = Haematoxylin&Eosin, α-SMA = alpha smooth muscle actin. All stainings were performed on paraffin embedded sections and with AR.

funnel-like dilated part of the ureter in the kidney. Functionally, the renal pelvis collects the urine from the calyces and funnels it into the ureter. Similar to the findings for the glomeruli and the Bertin columns (Fig. 11), the DAB stained paraffin sections show the typical structures well for collagen I, while collagen III is stained only very weakly (Fig. 12A). The corresponding cryosections are a bit less distinctive than the paraffin sections; although there is a higher contrast, the voids are larger, implying that some of the membranes had gone lost during processing. The standard staining H&E also depicts the typical structures of the pelvis very well, with small voids being lined with the urothelium. As for the immunofluorescently stained sections, they do not show the substructures of the pelvis as well as the DAB stained sections. Areas that are collagen I or collagen III positive are depicted only as spotty accumulations of green colour, without representing the substructures of the pelvis nearly as well as the DAB stained sections. Ki67 is again depicting the nuclei of proliferating cells quite nicely, for both the paraffin and cryosections, respectively: both showing acceptable to high contrast to the surrounding tissue. The PAR-2 stained sections show the voids for urine collections well, with the epithelial cells and/or the lamina propria in brown colour while the rest of the cells in the connective tissue is PAR-2 negative. Such findings are shown also in Fig. 11B at higher magnification, where the PAR-2 positive staining can be attributed to the cells forming the urothelium.

Furthermore, an excerpt of a calix, with blood vessels and tubuli is depicted in Fig. 13. As found in previous figures, paraffin sections stained chromogenic for collagen I and III can be judged superior compared with both, the corresponding cryosections and the corresponding immunofluorescently stained paraffin sections, respectively. While the collagen I positive areas in the paraffin sections with DAB staining depict the calix structures with the tubuli and some arteries very well, the collagen III staining intensity in subsequent sections is weaker at the corresponding location, but for both, collagen I and collagen III, respectively, it is precise and distinct from the (micro) environment. The corresponding cryosections have a too intensive colour; the brown is dark brown and there are slurries of colour around the margins of the substructures, provoking the impression of not really seeing the tiny ramifications that are in contrast well recognized in the paraffin sections. However, the big voids attributed to the calices can be seen well in all the stainings and in both, paraffin and cryosections.

With regard to immunofluorescent staining, in the panels selected here, only the fibronectin and α-SMA stained paraffin sections are usable to differentiate between arteries' and venules' composition in their vessel walls; the cryosections do not show it that distinctively than the paraffin sections.

3.7. Conclusive remarks on immunohistochemistry of the rabbit kidney tissue

The morphology of the rabbit kidney tissue with its different building blocks and extracellular matrix composition can be very well visualized using different immunohistochemical approaches besides the simple but very valuable traditional HE staining. We have discussed cryopreservation compared to formalin fixation and paraffin embedding as well as differences after an antigen retrieval step. It has to be emphasized that immunohistochemical staining of cryosections led in most cases to very well stained sections; with only ki67 that did not work well due to unspecific staining, leading to an overestimation of proliferating cells. Furthermore, we were able to elucidate main proteins making up the renal cortex, the medulla, the calices, the pelvis, glomeruli and Bertin columns in the natural, naïve rabbit kidney tissue. Interestingly and open for further interpretation and comparison to pathological states, the mesangial cells of the glomeruli were PAR-2 positive in the healthy kidney. Moreover, while the cells making up the distal convoluted tubuli were also PAR-2 positive, there was a complete absence of PAR-2 staining in the proximal tubuli of the renal corpuscle. This overview of histological and immunohistological staining might be used for preclinical studies using the rabbit kidney model, acting as baseline images of healthy tissue. Images of diseased kidney tissue can then prospectively be compared to the here presented images.

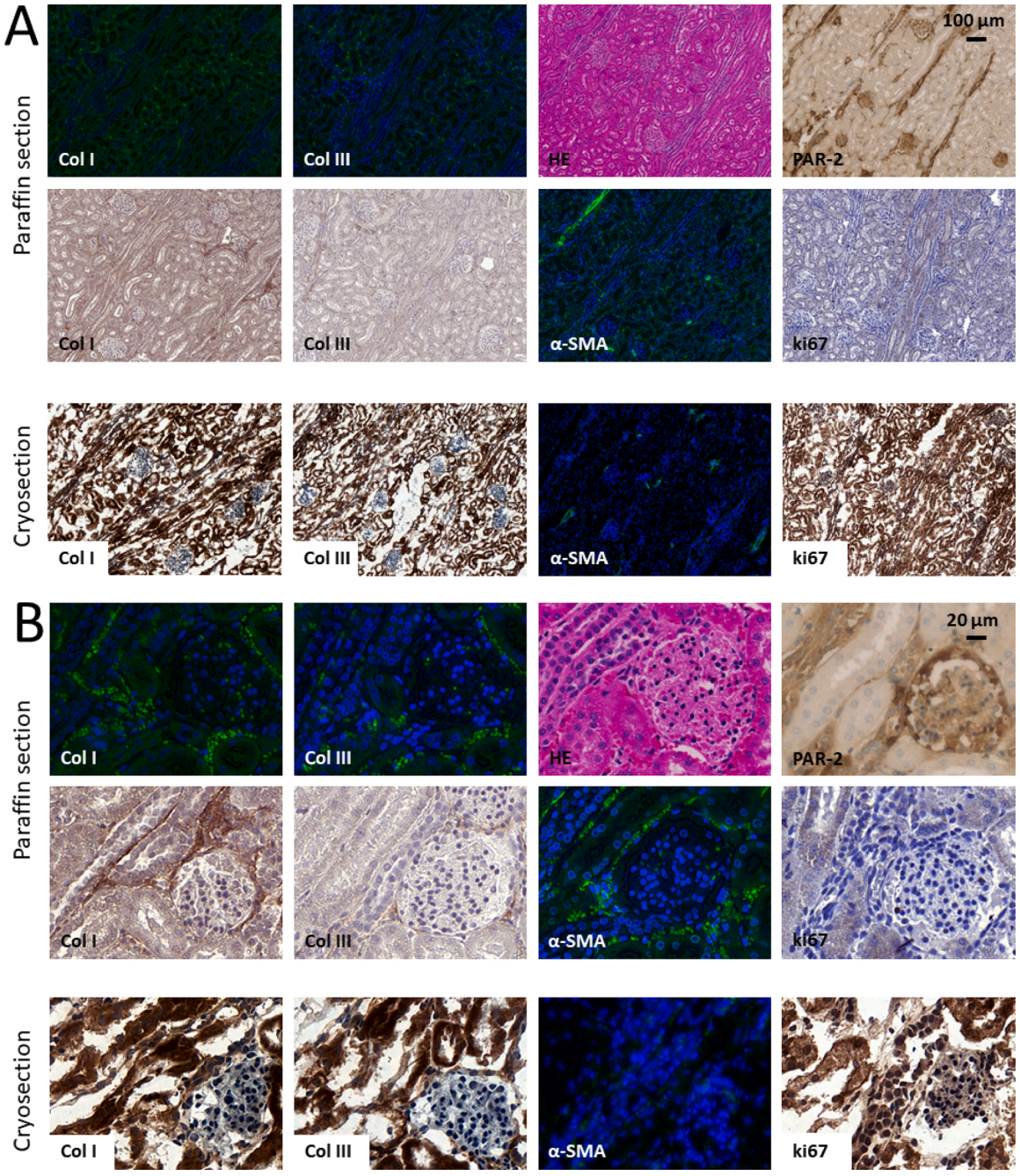

Fig. 11. Glomeruli and Bertin columns in detail in a series of different stainings for different magnifications (A and B) and for paraffin sections as well as cryosections. *Key*: Col = Collagen, Fn = Fibronectin, α-SMA = alpha smooth muscle actin, ki67 = proliferation marker ki67, PAR-2 = protease activated receptor-2, HE = Haematoxylin&Eosin. If not otherwise stated, all stainings were performed with AR on paraffin section.

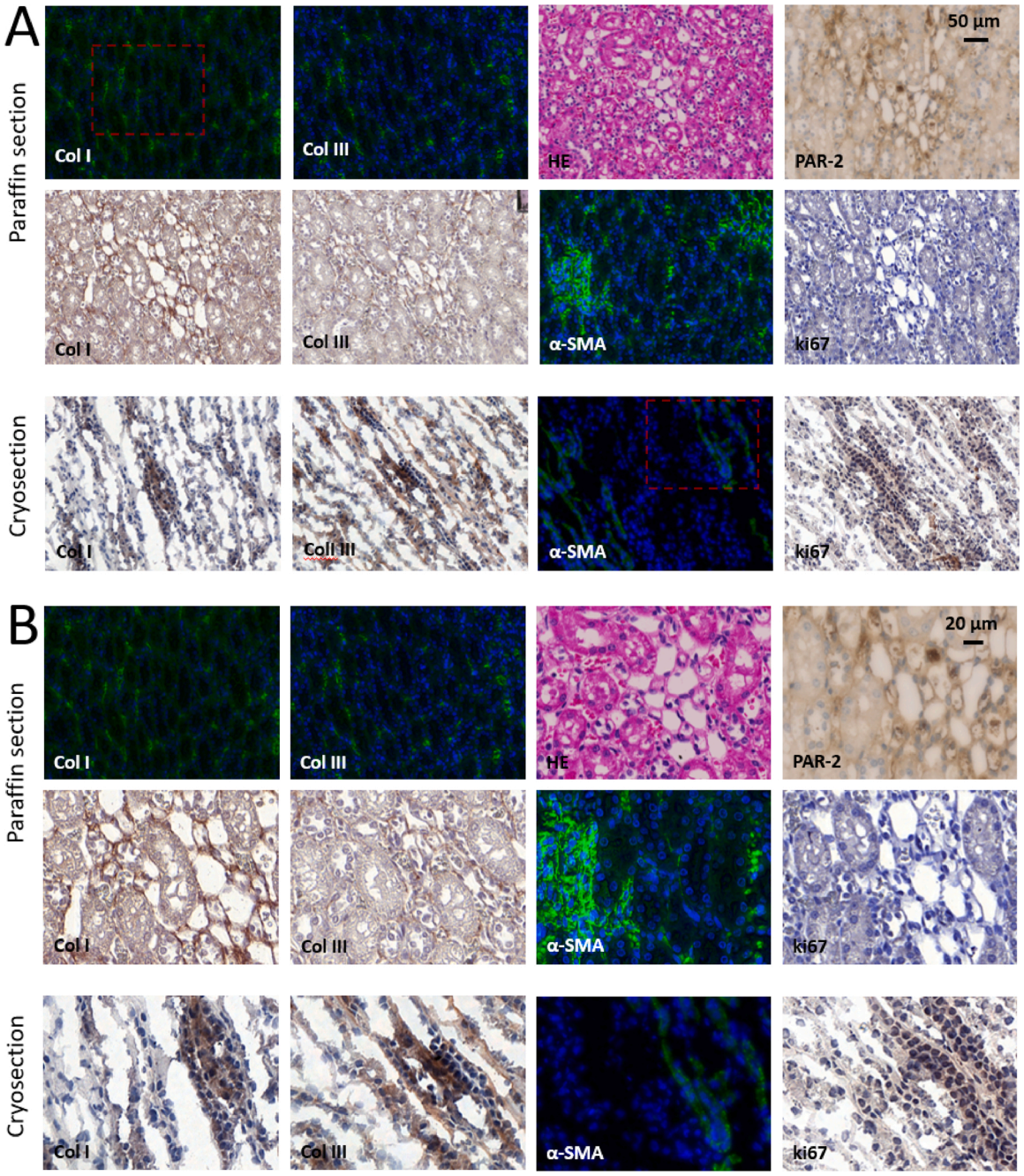

Fig. 12. Pelvis in detail in a series of different stainings for different magnifications (A and B) and for paraffin sections as well as cryosections. *Key*: Col = Collagen, Fn = Fibronectin, α-SMA = alpha smooth muscle actin, ki67 = proliferation marker ki67, PAR-2 = protease activated receptor-2, HE = Haematoxylin&Eosin, If not otherwise stated, all stainings were performed with AR on paraffin section.

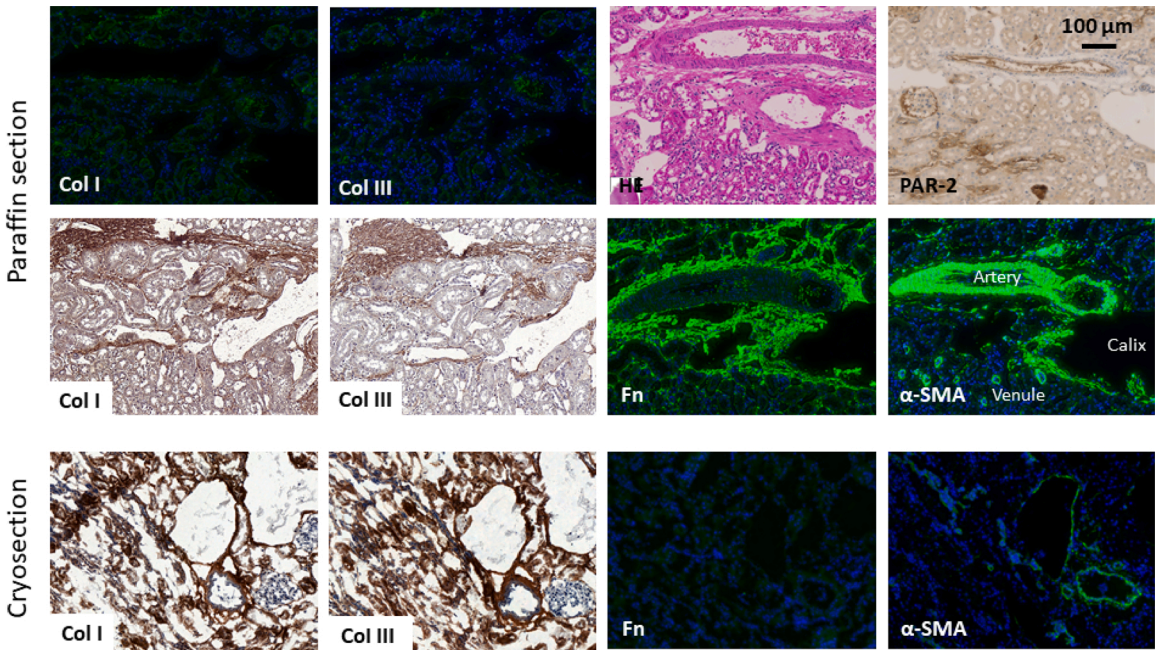

Fig. 13. Calix, blood vessels and tubuli in detail in a series of different stainings for the same magnification and for paraffin sections as well as cryosections. *Key*: Col = Collagen, Fn = Fibronectin, α-SMA = alpha smooth muscle actin, ki67 = proliferation marker ki67, PAR-2 = protease activated receptor-2, HE = Haematoxylin&Eosin. If not otherwise stated, all stainings were performed with AR on paraffin section.

Author contributions

GMB performed IHC stainings, imaged all sections and composed all figures. DMH gave input on PAR-2 staining. MC, JB and PG supervised the study. JB provided funding, wrote the manuscript and supervised the study.

Declaration of Competing Interest

The authors report no declarations of interest.

Acknowledgements

We thank the Hartmann Müller Foundation, Zürich, for financial support. We thank Flora Nicholls for kidney extraction from the cadaver rabbit. We thank Dr Olivera Evrova for her help with IHC protocol establishement and slide scanner management. Prof. Reto A. Schüpbach is kindly acknowledged for his input during discussions. Furthermore, we thank Ines Kleiber-Schaaf and Andrea Garcete-Bärtschi for their help with tissue sections and HE staining. We thank Silvia Behnke from Sophistolab, Switzerland, for PAR-2 immunohistochemical staining. We thank the Hartmann Mül.

Appendix A. Supplementary data

Supplementary material related to this article can be found, in the online version, at doi:https://doi.org/10.1016/j.acthis.2021.151701.

References

Alpers, C.E., Hudkins, K.L., Floege, J., Johnson, R.J., 1994. Human renal cortical interstitial cells with some features of smooth muscle cells participate in tubulointerstitial and crescentic glomerular injury. J. Am. Soc. Nephrol. 5 (2), 201–209.

Atwood, D.J., Brown, C.N., Holditch, S.J., Pokhrel, D., Thorburn, A., Hopp, K., Edelstein, C.L., 2020. The effect of trehalose on autophagy-related proteins and cyst growth in a hypomorphic Pkd1 mouse model of autosomal dominant polycystic kidney disease. Cell. Signal. 75, 109760. https://doi.org/10.1016/j.cellsig.2020.109760.

Beach, T.E., Prag, H.A., Pala, L., Logan, A., Huang, M.M., Gruszczyk, A.V., Martin, J.L., Mahbubani, K., Hamed, M.O., Hosgood, S.A., Nicholson, M.L., James, A.M., Hartley, R.C., Murphy, M.P., Saeb-Parsy, K., 2020. Targeting succinate dehydrogenase with malonate ester prodrugs decreases renal ischemia reperfusion injury. Redox Biol. 36, 101640 https://doi.org/10.1016/j.redox.2020.101640.

Boukhalfa, G., Desmoulière, A., Rondeau, E., Gabbiani, G., Sraer, J.D., 1996. Relationship between alpha-smooth muscle actin expression and fibrotic changes in human kidney. Exp. Nephrol. 4 (4), 241–247.

Cianciolo, G., Capelli, I., Cappuccilli, M., Scrivo, A., Donadei, C., Marchetti, A., Rucci, P., La Manna, G., 2017. Is chronic kidney disease-mineral and bone disorder associated with the presence of endothelial progenitor cells with a calcifying phenotype? Clin. Kidney J. 10 (3), 389–396. https://doi.org/10.1093/ckj/sfw145.

Cunningham, M.A., Rondeau, E., Chen, X., Coughlin, S.R., Holdsworth, S.R., Tipping, P. G., 2000. Protease-activated receptor 1 mediates thrombin-dependent, cell-mediated renal inflammation in crescentic glomerulonephritis. J. Exp. Med. 191 (3), 455–462. https://doi.org/10.1084/jem.191.3.455.

El Eter, E.A., Aldrees, A., 2012. Inhibition of proinflammatory cytokines by SCH79797, a selective protease-activated receptor 1 antagonist, protects rat kidney against ischemia-reperfusion injury. Shock 37 (6), 639–644. https://doi.org/10.1097/SHK.0b013e3182507774.

Ghayor, C., Weber, F.E., 2018. Osteoconductive microarchitecture of bone substitutes for bone regeneration revisited. Front. Physiol. 9, 960. https://doi.org/10.3389/fphys.2018.00960.

Karami, M., Owji, S.M., Moosavi, S.M.S., 2020. Comparison of ischemic and ischemic/reperfused kidney injury via clamping renal artery, vein, or pedicle in anesthetized rats. Int. Urol. Nephrol. https://doi.org/10.1007/s11255-020-02611-x.

Kuloglu, T., Dabak, D.O., 2009. Determination of ghrelin immunoreactivity in kidney tissues of diabetic rats. Ren. Fail. 31 (7), 562–566. https://doi.org/10.1080/08860220903050405.

Meier Bürgisser, G., Evrova, O., Heuberger, D.M., Calcagni, M., Giovanoli, P., Buschmann, J., 2020. Delineation of the healthy rabbit lung by immunohistochemistry – a technical note. Acta Histochem. 151648. https://doi.org/10.1016/j.acthis.2020.151648.

Morla, L., Brideau, G., Fila, M., Crambert, G., Cheval, L., Houillier, P., Ramakrishnan, S., Imbert-Teboul, M., Doucet, A., 2013. Renal proteinase-activated receptor 2, a new actor in the control of blood pressure and plasma potassium level. J. Biol. Chem. 288 (14), 10124–10131. https://doi.org/10.1074/jbc.M112.446393.

Moussa, L., Apostolopoulos, J., Davenport, P., Tchongue, J., Tipping, P.G., 2007. Protease-activated receptor-2 augments experimental crescentic glomerulonephritis. Am. J. Pathol. 171 (3), 800–808. https://doi.org/10.2353/ajpath.2007.061155.

Prochnicki, A., Amann, K., Wegner, M., Sock, E., Pfister, E., Shankland, S., Pippin, J., Daniel, C., 2018. Characterization of glomerular Sox9(+) cells in anti-glomerular basement membrane nephritis in the rat. Am. J. Pathol. 188 (11), 2529–2541. https://doi.org/10.1016/j.ajpath.2018.07.023.

Saeed, M.I., Nicklas, R.D., Kumar, V., Kapoor, R., Gani, I.Y., 2020. Severe intraoperative anaphylaxis related to thymoglobulin during living donor kidney transplantation. Antibodies (Basel, Switzerland) 9 (3). https://doi.org/10.3390/antib9030043.

Salguero, F.J., Mekonnen, T., Ruiz-Villamor, E., Sanchez-Cordon, P.J., Gomez-Villamandos, J.C., 2001. Detection of monokines in paraffin-embedded tissues of

pigs using polyclonal antibodies. Vet. Res. 32 (6), 601–609. https://doi.org/10.1051/vetres:2001103.
Saratlija Novakovic, Z., Glavina Durdov, M., Puljak, L., Saraga, M., Ljutic, D., Filipovic, T., Pastar, Z., Bendic, A., Vukojevic, K., 2012. The interstitial expression of alpha-smooth muscle actin in glomerulonephritis is associated with renal function. Med. Sci. Monit. 18 (4), Cr235–240. https://doi.org/10.12659/msm.882623.
Sharma, R., Waller, A.P., Agrawal, S., Wolfgang, K.J., Luu, H., Shahzad, K., Isermann, B., Smoyer, W.E., Nieman, M.T., Kerlin, B.A., 2017. Thrombin-induced podocyte injury is protease-activated receptor dependent. J. Am. Soc. Nephrol. 28 (9), 2618–2630. https://doi.org/10.1681/asn.2016070789.
Shi, S.R., Key, M.E., Kalra, K.L., 1991. Antigen retrieval in formalin-fixed, paraffin-embedded tissues: an enhancement method for immunohistochemical staining based on microwave oven heating of tissue sections. J. Histochem. Cytochem. 39 (6), 741–748. https://doi.org/10.1177/39.6.1709656.
Shi, S.-R., Liu, C., Taylor, C.R., 2006. Standardization of immunohistochemistry for formalin-fixed, paraffin-embedded tissue sections based on the antigen-retrieval technique: from experiments to hypothesis. J. Histochem. Cytochem. 55 (2), 105–109. https://doi.org/10.1369/jhc.6P7080.2006.
Shi, S.-R., Shi, Y., Taylor, C.R., 2011. Antigen retrieval immunohistochemistry: review and future prospects in research and diagnosis over two decades. J. Histochem. Cytochem. 59 (1), 13–32. https://doi.org/10.1369/jhc.2010.957191.
Siddiqui, A.Z., Bhatti, U.F., Deng, Q., Biesterveld, B.E., Tian, Y., Wu, Z., Dahl, J., Liu, B., Xu, J., Koike, Y., Song, J., Zhang, J., Li, Y., Alam, H.B., Williams, A.M., 2020. Cl-amidine improves survival and attenuates kidney injury in a rabbit model of endotoxic shock. Surg. Infect. (Larchmt.). https://doi.org/10.1089/sur.2020.189.
Siegenthaler, B., Ghayor, C., Ruangsawasdi, N., Weber, F.E., 2020. The release of the bromodomain ligand N,N-dimethylacetamide adds bioactivity to a resorbable guided bone regeneration membrane in a rabbit calvarial defect model. Materials (Basel) 13 (3), 501. https://doi.org/10.3390/ma13030501.
Tang, W.W., Ulich, T.R., Lacey, D.L., Hill, D.C., Qi, M.Y., Kaufman, S.A., Van, G.Y., Tarpley, J.E., Yee, J.S., 1996. Platelet-derived growth factor-BB induces renal tubulointerstitial myofibroblast formation and tubulointerstitial fibrosis. Am. J. Pathol. 148 (4), 1169–1180.
Tekçe, H., Aktaş, G., Öztürk, S., 2013. A distal (type 1) renal tubular acidosis case that mimic coronary ischemia. Ren. Fail. 35 (9), 1289–1291. https://doi.org/10.3109/0886022x.2013.820662.
Vesey, D.A., Suen, J.Y., Seow, V., Lohman, R.J., Liu, L., Gobe, G.C., Johnson, D.W., Fairlie, D.P., 2013. PAR2-induced inflammatory responses in human kidney tubular epithelial cells. Am. J. Physiol. Renal Physiol. 304 (6), F737–750. https://doi.org/10.1152/ajprenal.00540.2012.
Wang, Z., Li, M.X., Xu, C.Z., Zhang, Y., Deng, Q., Sun, R., Hu, Q.Y., Zhang, S.P., Zhang, J. W., Liang, H., 2020. Comprehensive study of altered proteomic landscape in proximal renal tubular epithelial cells in response to calcium oxalate monohydrate crystals. BMC Urol. 20 (1), 136. https://doi.org/10.1186/s12894-020-00709-z.